University of Dundee

School of Engineering, Physics and Mathematics

Department of Civil Engineering

DAM-BREAK IMPACT ON SUPPORTS OF COASTAL STRUCTURES

By

Callum Phin

Honours Project Thesis

Under the Supervision of Dr Masoud Hayatdavoodi

March 2018

Abstract

This thesis will investigate the lateral forces acting on a vertical structure due to a hydraulic bore resulting from the instantaneous break of a dam. The lateral forces imposed by a hydraulic bore are of significance importance in the design of coastal structures. However, bore-structure interaction is not fully understood. By use of the Navier-Stokes solver interFoam of the OpenFOAM package coupled with a volume of fluid scheme for phase interface capturing the simulation of a two-dimensional dam-break is modelled. The CFD computations of the effects of three parameters on the lateral forces of a vertical structure are presented and discussed. Peak force was shown to increase as initial dam height and structure height increased. Structure length appeared to have no influence in peak force, in the cases considered.

Contents

List of figures

List of tables

CHAPTER ONE
INTRODUCTION

A tsunami is a series of ocean waves typically caused by tectonic displacements in the ocean. They are rare natural disasters with an estimated return period of around 100 years for a tsunami of 25 m wave heights (Kulikov et al, (2005). Despite their infrequency, tsunami can generate hydraulic bores that propagate onshore causing catastrophic damage to coastal structures and endangering the lives of inhabitants.

In 2004, one of the strongest earthquakes in the past century struck off the coast of the island of Sumatra. This triggered an Indian Ocean tsunami which took the lives of 283,100 inhabitants across Indonesia, Sri Lanka, India, Thailand, Somalia, Maldives, Malaysia and several others (Wang & Liu 2006). In 2009, an earthquake south of the Samoa Islands in the southcentral Pacific triggering a tsunami. The tsunami caused 189 fatalities and considerable damage across the Samoa Islands and in the Tonga archipelago (Okal et al. 2010). Bores resulting from dam-breaks have also been responsible for numerous loss of life, perhaps most notably, the Malpasset dam-break of 1959. The collapse killed 421 people, resulting in the first legislation for dam-break risk analysis within Europe, during 1968 (Hervouet & Petitjean 1999).

The devastation of such events only highlights the importance for engineers to understand the impact forces generated by hydraulic bores. Many coastal structures undergo severe structural damage when subjected to these lateral forces. Unlike seismic and wind loads, hydraulic bores will generally have the most impact on the ground floor of a structure. These loads will induce failures in ground floor supports. By the investigation of such loads, coastal structures may be sufficiently designed to withstand them. One method used to research hydraulic bores involves simulation of a dam-break. Based on analogies made by Chanson (2006), dam-break waves correlate to those of a tsunami, and vice versa.

This work investigates various dam and structure configurations in order to achieve a better understanding of the dam-structure relationships relating to impact loads. The dam-break induced bore is generated using the open source computational fluid dynamics (CFD) software OpenFOAM. The package uses a finite volume to solve Navier-Stokes equations with a volume of fluid (VOF) scheme for free-surface tracking of multi-phase flows.

1.1 Aims and objectives

The aim of this study was to analyse the forces on a vertical structure by a dam-break induced hydraulic bore.

To meet this aim the following objectives were set:

1. To review available literature on hydraulic bores and bore-structure interaction.
2. To carry out simulations involving a dam of varying initial water heights to determine the effect of initial water height on impact load.
3. To carry out simulations involving a structure of varying height, then length, to determine the effect of structure size on impact load.

1.2 Thesis structure

A review of the background literature relevant to this study is presented in Chapter 2. This chapter highlights the need for the analysis of hydraulic bore behaviour and goes on to introduce common areas of study. The origin of the dam-break problem and analytical solutions typically used in experimental and numerical models are discussed. The initial stages, characteristics, induced forces and the use of numerical models in the study of hydraulic bores are described. Particular emphasis is placed on the use of numerical methods. The chapter ends with a summary of areas that require additional investigation.

Chapter 3 and 4 are concerned with the computational solution of the dam-break problem. Chapter 3 presents the governing equations, the model used in the discretisation of the governing equations and the employed method of surface tracking. Chapter 4 describes the computation solution in detail, including information regarding the software, mesh, model and validation of the software.

Chapter 5 and 6 investigate the effects of initial dam height, structure height and structure length. Chapter 5 concentrates on the test case configuration and description of the variables of each problem. The results are presented and discussed in Chapter 6. Bore profile, peak impact force and moment of peak impact are among the characteristics analysed.

Chapter 7 summarises the key conclusions from this study and makes suggestions for future research.

CHAPTER TWO
LITERATURE REVIEW

2.1 Introduction

This literature review will highlight the importance in the investigation of dam-break problems. The focus will be dam-break waves and tsunami induced bores. Previous investigations into of the effect of basic parameters on bore characteristics will be identified. Induced forces of different hydraulic bores will be discussed, including the method of approach and the conclusions made.

2.2 Importance of dam-break flow study

The dam-break flow has been a topic of significant research interest due to both practical and academic interests. Chanson (2006) made analogies between the instantaneous free surface flow profiles of a dam-break flow and a tsunami induced bore on a horizontal bed. The study compared dam-break analytical results with observed tsunami surge data, observing flow similarities. The study enables results of dam-break problems to be applied to tsunami induced hydraulic bores, and vice versa.

Dam failures motivated basic studies on the dam-break wave. Failures cause huge economic loss and release large quantities of water. The 1975 Banqiao Dam-break alone flooded tens of kilometres of land and killed an excess of 85,000 people (Si 1998). Despite the importance of historic dam failures, tsunami have posed a greater risk in recent years. In 2004, an earthquake with magnitude 9.3 on the Richter scale off the northern Sumatra generated huge tsunami waves that led to widespread catastrophes in many countries bordering the Indian Ocean (Choi et al. 2006). The event took 283,100 lives and caused immense economic loss (Wang and Liu 2006). In 2006, another tsunami was triggered off the southern coast of Java, Indonesia by an earthquake with magnitude 7.7 on the Richter scale. The tsunami resulted in over 730 casualties (Lavigne et al. 2007). A further 189 were killed across Tonga, Samoa and American Samoa by the 2009 South Pacific tsunami (Okal et al. 2010). The devastating effects of these events only emphasises the requirement to better understand the behaviour and forces of hydraulic bores.

2.3 Hydraulic bore

As waves propagates towards a shoreline and water depth decreases, their wave height increases while velocity decreases. When the water depth is approximately equal to the incident wave height the waves break and run up shore in the form of a hydraulic bore. Following a dam-break, or tsunami, the generated hydraulic bores are fast moving and have the potential to be dangerous to the surrounding areas. Flow depth and flow velocity are two of the main characteristics that define a hydraulic bore.

2.3.1 Flow depth

Ritter (1892) introduced a theoretical description to explain the flow caused by the instantaneous failure of a dam in a rectangular and horizontal channel problem. The solution assumed an infinite length for both reservoir and channel and a frictionless channel. The effects of hydraulic resistance were included by Dressler (1952) and Whitham (1955). Stoker (1957) extended the solution to the case of wet-bed condition downstream of the dam. To this day, Ritter's solution for dry-bed channels and Stoker's solution wet-bed channels are used for comparison with experimental and numerical investigations.

Regarding experimental and numerical investigations, a common test case is the idealised two-dimensional problem of the instantaneous removal of a barrier between two bodies of water. In reality, the removal of a barrier is never instantaneous. Stansby et al. (1998) investigated the initial stages of dam-break flow after the release of a barrier. A mechanical pulley system was implemented to keep the release constant between experiments where dry- and wet-bed cases were investigated at two scales. In the short time before bore formation, a jet-like phenomena was observed. However, free surface profiles showed close agreement with Stoker's analytical solution after the formation of a bore. The study allows the jet-like phenomena to be considered insignificant for cases where the formation of a bore is present.

It is important to remember most analytical and experimental studies consider simple or idealised channels. Channel characteristics such as roughness and geometry will play key roles in the behaviour of dam-break flows. The effect of channel roughness is an important aspect for estimating how bores will behave. Varying roughness in a straight channel was investigated by Dressler (1954) and Bell et al. (1992). Dressler (1954) compared measured results to analytical solutions from Dressler (1952) and Whitham (1955) for smooth, intermediate and rough channels. Bell et al. (1992) conducted tests with a smooth and rough channel bottom.

Both studies observed a more inclined bore face for an increase in the Manning roughness coefficient. Different geometries were investigated by Frazão & Zech (2002), Miller and Chaudhry (1989) and Bell et al. (1992). Frazão & Zech (2002) measured the flow profile in channels with a sharp 90 ° bend. Miller & Chaudhry (1989) and Bell et al. (1992) also measured the flow profile but for a channel with a 180 ° bend. All works consisting of a non-straight channel observed superelevation due to reflection.

2.3.2 Flow velocity

Several works have measured the velocity of dam-break flow (e.g. Fraccarollo & Toro 1995; Stansby et al. 1998; Frazão & Zech 2002; Janosi et al. 2004; Eaket et al. 2005). Fraccarollo & Toro (1995) implemented current meters to record velocity at points throughout the channel. Despite experiencing difficulty in the stabilisation of current meters, the results were in agreement with their numeric model. Velocity was shown to fluctuate with time across each probe. The direct measurement of velocity, as in this case, is rare. A more typical method of measuring the velocity of dam-break flow is by various image analysis techniques. Stansby et al. (1998) and Janosi et al. (2004) used fast-shutter cameras to investigate dry- and wet-bed conditions. Frazão & Zech (2002) studied a channel with a single 90 ° bend by tracking small tracers in the flow. Eaket et al. (2005) investigated the viability of video stereoscopy. However, due to the nature of these techniques, difficulties often arise measuring data close to the channel bed. Thus, results are often of varied success.

2.4 Bore-structure interaction

Historically, analytical and experimental research to quantify bore characteristics and forces due to hydraulic bores has been widely carried out. Snodgrass et al. (1951) noticed that hydraulic bores imposed larger hydrodynamic horizontal forces on a vertical component compared to waves breaking at the component. Cumberbatch (1960) presented a solution for the impact of a two-dimensional fluid wedge on a vertical wall. Cross (1967) studied surges advancing into still water and their impact forces on vertical walls, using the same method as Cumberbatch (1960).

The study of bore-structure interaction is majorly limited to the case where the flow is restricted to one side of the structure (e.g. Ramsden & Raichlen 1990; Ramsden 1993; Ramsden 1996; Zhou et al. 1999). Ramsden & Raichlen (1990) and Ramsden (1993, 1996) conducted a comprehensive experimental investigation of the interaction of solitary waves, bores and surges

on a dry-bed with a vertical wall. Ramsden & Raichlen (1990) investigated the effects of bore height and velocity on the forces on a vertical wall. It was observed that the maximum measured force occurred after the maximum runup for all conditions of the study. Ramsden (1993) found the force on a vertical wall due to the impingement of a bore on a mildly sloping bed is equivalent to the force produced by a bore of constant volume on a horizontal bed. Thus, implying studies involving a horizontal channel can be used to estimate the loads expected from bores propagating on slopes ranging up to 0.02 m/m. Ramsden (1993, 1996) both found the vertical accelerations of the flow reduce the force predicted from a hydrostatic condition. The measured forces on a vertical wall by Ramsden under predict the theories of Stoker (1957) and Cross (1967) by up to 40 % and 50 %, respectively. Robertson et al. (2013) used a large wave flume to experimentally quantify the lateral load applied to a vertical wall when subjected to tsunami bores. Hydrodynamic forces on the wall structure were found to be much larger than typical lateral design forces. Zhou et al. (1999) also experimentally measured dam-break impact on a vertical wall. Pressure transducers were located on the impact plate and probes were placed across the channel to track water height. As with similar experimental setups, a flap restricting the movement of water was lifted allowing water in the dam-area to move in to the flow area. The experiments were not fully reproducible and very small changes in the initial conditions showed clear differences in results. In spite of the lack of reproducibility, the configuration and results have since been used as a benchmark for comparison with numerical results (e.g., Colicchio et al. 2002; Nielsen, 2003; Abdolmaleki et al. 2004; and Ji et al. 2013).

Palermo et al. (2009) and Nistor et al. (2010) investigated the individual force components of a tsunami-induced bore. Palermo et al. (2009) found that drag forces were found to be the largest force component for smaller impoundment depths, whilst surge and runup were more critical for the larger impoundment depths. Runup force was found to be greater than surge force for all bore depths. Maximum force acted at approximately 40 % of the surge height during the initial impact. Nistor et al. (2010) considered the loading combinations of drag, debris and surge force from a tsunami-induced bore. It was concluded the width of exposed surfaces affects the magnitude of total force exerted on a structure. The use of breakaway or flexible walls at the lower level was proposed as a method to reduce lateral forces. Pacheco and Yeh et al. (2005) predicted individual shear walls perpendicular to tsunami flow have the potential to fail and lead to progressive collapse of the building. It was also predicted a structure with relatively thin walls to support gravity and lateral loads would likely perform poorly

during a tsunami event. Hydrodynamic and impact forces to be the most probable forces for near-shoreline structures.

Yeh (2006) and Nouri et al. (2010) acknowledged the implications of shape on the forces imposed on that structure. Yeh (2006) computed temporal and spatial variations of water depth and flow velocity of tsunami runup on a uniformly sloping beach. Using analytic and numeric solutions an envelope curve of the maximum tsunami-force distribution in the runup zone was established. The method can be used to compute the actual force on a specific object by application of its drag coefficient. Nouri et al. (2010) experimentally studied the pressures and forces exerted on three free-standing structures with square, diamond and circular cross-sections for different configurations. These included upstream obstacles and debris impact. The structure of square cross section experienced the greatest pressure.

Few studies have investigated the flow against an isolated obstacle (e.g. Gómez-Gesteira & Dalrymple 2004; Frazão & Zech 2007). Gómez-Gesteira & Dalrymple (2004) investigated the forces on a tall structure from a dam-break. Vertical distributions of force exerted on the front of the structure were found to be closer to the bottom of the structure for a dry-bed condition than a wet-bed condition.

2.5 Use of numerical modelling for dam-break problems

An accurate numerical model allows simple and complex problems to be studied efficiently, with exact reproducibility. Regarding the dam-break problems, numerical models have become a popular alternative to analytical and experimental methods. This is likely due to the incapability of analytical solutions to deal with complex geometries and the difficulty of recording data and the reproducibility of laboratory experiments methods. Currently, the extent of numerical modelling majorly consists of the validation of various numerical models by comparison with analytical solutions and experimental results (Colicchio et al. 2002; Ji et al. 2013; Zhainakov & Kurbanaliev 2013).

An abundance of numerical models solving the shallow water equations by methods of finite element, finite difference and finite difference have been employed in dam-break problems (Bellos & Sakkas 1987; Fennema & Chaudhry 1987; Fraccarollo & Toro 1995; Wang et al. 2000 Valiana et al. 2002; Frazão & Zech 2007).

Recently, models solving the Navier-Stokes equations have been used for two-dimensional dam-break problems (Yue et al. 2003; Abdolmaleki 2004; Biscarini et al. 2010; La Rocque et al. 2013). LaRocque et al. (2013) used a Navier-Stokes equations solver, with the volume of fluid (VOF) method for surface tracking, to successfully track the flow profile for turbulent test cases. The numerical data was compared with data experimentally obtained within the same paper. Results were comparable. Thus, proposing numerical modelling with a VOF approach as a reliable method of simple and complex dam-break flow prediction. Similarly, to LaRocque, Zhainakov & Kurbanaliev (2013) solved the Navier-Stokes equations with a volume of fluid method for surface tracking to investigate a number of dam-break problems, including free surface elevation. Despite inaccuracies involving the impingement of reverse waves moving oppositely to the main flow onto the free surface, the OpenFOAM model generally produced more accurate results than other CFD packages.

The smoothed particle hydrodynamics model, developed by Gingold & Monaghan (1977), has also been applied to numerical models to predict dam-break flow. Despite being developed for astrophysics, the model has been successfully applied to wave propagation (Monaghan and Kos 1999) and wave impact (Gómez-Gesteria & Dalrymple 2004; Gómez-Gesteria et al. 2005).

Regarding geometry, the experimental setup used by Zhou et al. 1999 appears to be a good standard Colicchio et al. (2001) presented a comparative study of the dam-break problem using three different numerical methods. Nielson (2003) studied the pressure on the downstream wall of the mesh. Abdolmaleki et al. (2004) and Ji et al. (2013) studied the averaged impact pressure over an area corresponding to the pressure gauge. The results both agreed with experimental measurements of Zhou et al. (1999) for the initial impact.

2.6 Summary

Whilst analytical solutions from Dressler (1952), Whitham (1955) and Stoker (1957) define dam-break flow for idealised, dry- and wet-bed channels. The behaviour of dam-break flows are yet to be fully understood. Laboratory experiments investigate the basic effects of parameters, such as channel roughness (Dressler 1954) and geometry (Miller and Chaudhry 1989; Bell et al. 1992; Frazão & Zech 2002) on free surface profile. The velocity of flow was investigated in numerous studies with moderate success. The nature of recording the velocity by various image analysis techniques was generally implemented. This, alongside the difficulty changing geometry and reproducing exact initial conditions, has led to the increased interest in numerical models.

The majority of numerical computation work of dam-break flows concerns the validation of a numeric model (Colicchio et al. 2001; Ji et al. 2013). The experimental setup used by Zhou et al. (1999) is a common benchmark for use in numerical investigations (e.g., Colicchio et al. 2001; Nielsen, 2003; Abdolmaleki et al. 2004; and Ji et al. 2013). Thus, this configuration will be considered when defining the mesh in the present study.

Of the available computational fluid dynamics packages available, OpenFOAM is shown to be a valuable tool for the simulation of dam-break. Zhainakov & Kurbanaliev (2013) used the package to solve Navier-Stokes equations for dam-break problems. The results of the initial impact were in good agreement with experiments. The volume of fluid method, was implemented to track the free-boundary location. Both, Zhainakov & Kurbanaliev (2013) and LaRocque (2013) employed the Volume of Fluid method and concluded it a reliable approach for surface tracking.

Despite the numerous studies on dam-break problems, bore-structure interaction has not been as broadly investigated as other aspects. The most probable forces for near-shoreline structures are hydrodynamic and impact, according to Yeh et al. (2005). Most of the existing literature on bore-structure interaction investigates the impact loads of a hydraulic bore on a vertical wall (e.g. Ramsden 1996; Nielsen 2003; Abdolmaleki et al. 2004; Ji et al. 2013; Robertson 2013) Structural dimensions are rarely considered in dam-break problems. Of the limited research, experiments were carried out for a vertical structural element by Santo & Robertson (2010) and numerically for a tall structure by Gomez-Gesteira & Dalrymple (2004). It is clear the effects of hydraulic bores on free standing structures requires further investigation. Debris forces are acknowledged as contributory impact forces but will be ignored for the two-dimensional solution in this work.

CHAPTER THREE
THEORY

This section will provide an understanding of the computational fluid dynamics theory used in this study.

3.1 Governing equations

The Navier-Stokes equation governs the motion of fluid. It is obtained by the combination of the Cauchy's equation of motion and the constitutive equations.

The law of conservation of momentum is expressed in differential form by applying Newton's law of motion to an infinitesimal fluid element as

$$\rho \frac{\mathbf{dU}}{\mathrm{d}t} = \rho \mathrm{g} + \frac{\partial \tau_{ij}}{\partial x_j} \tag{1}$$

where $\rho \frac{\mathbf{dU}}{\mathrm{d}t}$ is the total acceleration per unit volume, ρg is the body force per unit volume and $\frac{\partial \tau_{ij}}{\partial x_j}$ is the i-component of the surface force per unit volume (Kundu & Cohen 2008). This is known as Cauchy's equation of motion. It holds for any continuum, solid or fluid, regardless of how the stress tensor τ_{ij} is related to the deformation field.

The relation between the stress and deformation in a continuum is called a constitutive equation. The constitutive equation can be written as

$$\tau_{ij} = -p\boldsymbol{\delta} + 2\mu \boldsymbol{e} \tag{2}$$

for the condition of the continuity equation

$$\nabla \cdot \mathbf{U} = 0 \tag{3}$$

where $-p\boldsymbol{\delta}$ is the stress that would exist at rest for directional vector $\boldsymbol{\delta}$, μ is the kinematic viscousity, $\boldsymbol{e}$ is the strain rate tensor vector and **U** is the velocity vector (Kundu & Cohen 2008).

By substituting the constitutive equation (Equation 2) into Cauchy's equation (Equation 1) and expanding the acceleration term, the Navier-Stokes equation for an incompressible, viscous fluid can be obtained as

$$\rho \frac{\partial(\mathbf{U})}{\partial t} + \rho \mathbf{U} \cdot \nabla \mathbf{U} = -\nabla \mathrm{p} + \mu \nabla^2 \mathbf{U} + \rho \mathbf{g}.\mathbf{x} \tag{4}$$

where **U** is the velocity vector, p is the dynamic pressure, μ is the kinematic viscousity, ρ is the density of the fluid, **g** is the gravity vector and **x** is the position vector (Kundu & Cohen 2008).

Assumptions made by the Navier-Stokes equation (Equation 4) are as follows: fluid is a continuum in order to satisfy Cauchy's equation; coefficient of bulk viscousity is equal to zero, thus, simplifying the constitutive equation; and viscousity μ is constant, i.e. temperature differences are small within the fluid.

Of the extensive literature available on fluid mechanics, Kundu & Cohen (2008) provides a thorough derivation of the conservation laws considered in this paper.

3.2 Finite volume

The governing equations are discretised using the finite volume model. Finite volume is one of the two models available for visualising a continuum fluid. The model makes use of a closed volume drawn within a finite region of the flow. It may be fixed in space with the fluid moving through it or as a region that moves with the fluid such that the same fluid particles are always inside it. The fundamental physical properties are applied to the fluid within the fixed volume. This allows the flow field to be analysed as a collective of smaller control volumes rather than the whole flow field at once. The fluid flow equations obtained by the application of the fundamental physical principles to a finite volume are in integral form. These equations can then be manipulated to obtain partial differential equations, providing the conservation form of the governing equations.

3.3 Volume of fluid

The key characteristic of VOF method is the employment of the phase fraction α. The phase fraction α provides a method to track the fluid-fluid interface. Simply, the method works by computing the fluid volume at each cell. Cells containing only one phase will have a phase fraction α equal to zero or unity. However, cells containing an interface will be of value between zero and one. Thus, as an idealised immiscible case is assumed, the interface between fluids can be located for a phase fraction α equal to a half. The phase fraction is calculated according to the equation, suggested by Hirt and Nichols (1981), as

$$\frac{\partial \alpha}{\partial t} + V \times \nabla \alpha = 0 \tag{5}$$

CHAPTER FOUR
COMPUTATIONAL SOLUTION

In this section, the software and conditions used in computations will be discussed. Model validation will bring the section to a close.

4.1 Software

The open source computational fluid dynamics software, Open Field Operation and Manipulation (OpenFOAM) is used to study the two-dimensional horizontal and vertical forces of a hydraulic bore on a structure. The solver *interFoam*, part of the OpenFOAM CFD Toolbox (OpenCFD 2007), was chosen for its capability to solve for two incompressible, isothermal immiscible fluids. The fluid-fluid interface is tracked using a Volume of Fluid (VOF) method approach, for post-processing.

4.2 Mesh

In OpenFOAM, all computations are three-dimensional with a single cell in the z-direction. To obtain a two-dimensional solution, the z-direction is set to be a single cell thick. The mesh is defined in the *blockMeshDict* file in the *system* directory, covered later in Section 4.3.3. For our mesh, six boundaries are defined: left, right, bottom, object, atmosphere and the front and back of the domain. The geometry of the mesh is defined by specifying vertices in Cartesian form. The atmosphere boundary type is defined as *patch*, the front and back as *empty* and the remainder as *wall*. The *patch* instruction creates a patch where there is no physical boundary, allowing fluid to flow in and out of the mesh. The *empty* instruction is utilised for the front and back planes of a two-dimensional geometry. Thus, equations and terms related to this direction, such as the front and back boundaries, will be ignored by the package. The front and back planes are specified as *frontBack* boundary. Finally, the *wall* instruction creates a physical boundary within the mesh. The mesh defined in *blockMeshDict* is non-uniform in this case with a degree of resolution higher around the object and lower in areas further from the object. Although smaller elements may be missed away from the object, the varying degree of resolution allows optimal results with minimal computational expense. Mesh boundary conditions are summarised in Table 1.

Table 1: Boundary conditions

Boundary	**Type**
left	*wall*
right	*wall*
bottom	*wall*
object	*wall*
atmosphere	*patch*
frontBack	*empty*

4.3 Model

The model is defined in three directories; initial time, constant, and system. This section will discuss all three in detail to provide an understanding of model used. All directories used in calculations can be found in the appendix.

4.3.1 Initial time

The initial conditions of the model are defined in the *0* directory. The directory contains three key files which define the model: phase fraction α, pressure p and velocity U. Due to the nature of the governing equations, it is necessary to specify the initial values of all dependant variables. The *internalField* is set to be uniformly zero for these files. In the phase fraction α file, this means to set default cells to contain air. The inclusion of a secondary fluid is specified in the constant directory, as shown in Section 4.3.3. For the pressure p and velocity U files, there is no motion until the moment of time t = 0. Therefore, it is assumed a diaphragm is present around the body of water until simulations begin at which point the column will be affected by gravitational acceleration.

The 0 directory is used to define parameter boundary conditions. The parameter conditions are summarised in Table 2. For a Newtonian fluid, a *noSlip* constraint is applied to wall boundary conditions i.e. assuming that the fluid will have zero velocity relative to the boundary. A *zeroGradient* condition is used setting the boundary value of said variable to the near-wall cell value. Thus, removing the pressure gradient at the boundary. The front and back planes have an *empty* boundary condition, as discussed in Section 4.2, the. Full definitions of all boundary conditions can be found in OpenCFD, (2007).

Table 2: Parameter boundary conditions

Boundary	**α**	**p**	**U**
leftWall	*zeroGradient*	*fixedFluxPressure*	*noSlip*
rightWall	*zeroGradient*	*fixedFluxPressure*	*noSlip*
lowerWall	*zeroGradient*	*fixedFluxPressure*	*noSlip*
object	*zeroGradient*	*fixedFluxPressure*	*noSlip*
atmosphere	*zeroGradient*	*totalPressure*	*pressureInletOutletVelocity*
frontBack	*empty*	*empty*	*empty*

4.3.2 Constant

The files in this directory define gravity, material properties and the simulation type. Firstly, for the file *g*, gravity is set as 9.81 m/s^2 in the downward y-direction. For file *transportProperties*, the physical properties of the fluids water and air are specified. Both fluids have a single valued kinematic viscousity so the transport model *Newtonian* is selected for each. The kinematic viscousity υ (*nu)*, density ρ (*rho)* of each fluid and the surface tension σ (*sigma*) of both fluids are summarised in Table 3. Finally, for the *turbulenceProperties* file, the simulation type is set to *laminar*.

Table 3: Fluid properties

Properties	**Value**	**Units**
Density of air ρ_a	1.225	kg/m^3
Density of water ρ_w	1000.00	kg/m^3
Kinematic viscousity of air υ_a	1.48E-06	m^2/s
Kinematic viscousity of water υ_w	1.00E-06	m^2/s
Surface tension σ	0.07	N/m

4.3.3 System

The *system* directory is used for setting parameters associated with the solution procedure. It contains the following files of importance: *blockMeshDict*, *setFieldsDict*, *controlDict*, *fvSchemes* and *fvSolution*. The *blockMeshDict* controls the mesh, as detailed previously in Section 4.2. The inclusion of water is defined in *setFieldsDict*. Here, the phase fraction *α* conditions are specified where unity is used for the water phase and zero is used for the air phase.

The *controlDict* includes the solver, run control parameters including start/end time, the frequency of data output and the presence of functions. The important aspects of *controlDict*

are as follows. The solver being used for two incompressible fluids is *interFoam*. The start time is set to be at 0, where the initial conditions are stored. All cases in this project run for 3.0 seconds, with calculations carried out every 0.0001 s and data recorded every 0.1 s. Two functions will be utilised in this model: *forces* to calculate the force on the object due to total pressure at time t; and, *freeSurface* to track the fluid-fluid interface at time t. The *forces* function uses the CFD Toolbox type forces to calculate the force on the patch *object*. Additionally, drag and lift forces are set in the x and y-direction, respectively. The *freeSurface* function uses the type *surfaces* to record the phase fraction α equal to 0.5, i.e., midway between the water phase and air phase.

The *fvSchemes* file includes the discretisation schemes used in the solution. The *interFoam* solver uses the multidimensional universal limiter for explicit solution (MULES) method to maintain boundedness of the phase fraction independent of underlying numerical scheme, mesh structure, etc. The sub-dictionary *divSchemes* setup is summarised in Table 4. Other discretised terms use commonly employed schemes such that the defaults of sub-dictionaries *ddtSchemes*, *gradSchemes* and *laplacianSchemes* are set to default *Euler*, *Gauss linear* and *Gauss linear corrected*, respectively. A full description of the discretisation schemes can be found in OpenCFD (2007).

The *fvSolutions* file contains information about the solvers to use for different parameters. Most importantly, a merged PISO-SIMPLE algorithm named PIMPLE is used for incompressible, unsteady flow. The phase fraction α solver is *smoothSolver*, with the smoother *symGaussSeidel* and a *tolerance* of $1e-08$. The pressure p solver is PCG, with a preconditioner of DIC and a *tolerance* of $1e-05$. The velocity U adopts the same solver as phase fraction α and has a *tolerance* of $1e-05$. The *relevantTolerance* is set to zero throughout *fvSolution*.

Table 4: Discretisation schemes

Term	**Discretisation scheme**
div(rhoPhi,U)	*linearUpwind grad(U)*
div(phi,alpha)	*vanLeer*
div(phirb,alpha)	*linear*
*div(((rho*nuEff)*dev2(T(grad(U)))))*	*linear*

4.7 Model validation

The intricacy of the OpenFOAM package can allow minor changes in configuration to produce major differences in results. Therefore, before the application of test cases, validation of the model is necessary.

4.7.1 Configuration

Regarding validation, a water column is held stationary by a retaining structure. At the initial moment of time, the rectangular column of incompressible fluid begins at rest. The liquid will induce a hydrostatic force on its container. This force will be calculated analytically and compared to the numerical solution retrieved from OpenFOAM in order to achieve acceptable results. Thus, verifying the package setup.

Test parameters are summarised in Table 5. Two initial water heights will be used in the validation of results. Figure 1 shows the configuration of the test model problem. The comparison between analytical results and the numerical solution must be comparable for future test cases in this work to be admissible. It is important to remember that total pressure is a result of both dynamic and static pressure. Though, for the simplicity of an analytical solution the configuration is defined such that the hydrodynamic pressure will equal zero.

Table 5: Software validation case parameters

Case	Water column height h (m)	Structure height H (m)
1	0.15	0.30
2	0.30	0.45

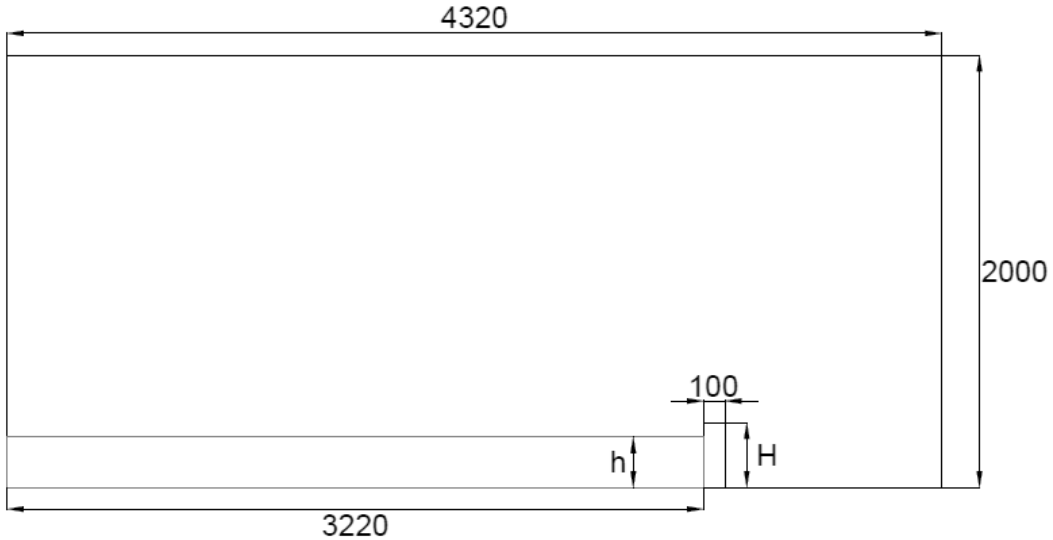

Figure 1: The configuration used in computations to validate OpenFOAM model (mm)

4.7.2 Analytical solution

This method calculates force due to hydrostatic pressure by analytical approach. The hydrostatic pressure at a given point within the fluid is given by

$$p_s(h) = \rho g h \tag{6}$$

where P_s is the hydrostatic pressure (N/m^2), ρ is the density of the fluid (kg/m^3), g is gravitational acceleration (m/s^2) and h is the depth from the surface (m). It is well known multiplying pressure P by area A of a face gives the total force F on that face. In a case such that pressure changes with depth, it is not enough to simply multiply function P_s by area. Instead, the function of hydrostatic pressure P_s must be integrated. Therefore, force can be derived as

$$F = w \int_0^h \rho g h \, dh \tag{7}$$

where F is the force (N) and h is the depth from the surface (m).

4.7.3 Numerical solution

Firstly, the boundaries of the object are created in the mesh to allow forces to be defined on the chosen faces; left, top and right. The numerical solution is obtained through the solver *interFoam*. Typically, only pressure is calculated by the solver. The use of the packages integrated forces library was implemented to calculate the loads on the object due to the pressure obtained in the solver. The total pressure p_T, as calculated in the pressure tool as utilised by *interFoam*, is given as

$$p_T = p_{ref} + \rho \mathrm{gh} + 0.5\rho|\mathrm{U}|^2$$

where p_{ref} is the reference pressure level (N/m^2) and U is the velocity (m/s) (OpenCFD 2007). The reference pressure is set to zero for all cases.

4.7.4 Validation

The results of both the analytical and numerical solutions are used to summarise the admissibility of the numerical solution. Table 6 compares the results from the cases stated in Section 4.7.1. The analytical and computational solutions are comparable, well within a ± 1% difference. Thus, future test case results in this work can be recognised as acceptable.

Table 6: Comparison of the analytical solution and numerical results from OpenFOAM model

Case	Analytical results (N)	Numerical solution (N)
1	110.36	110.36
2	441.45	441.38

CHAPTER FIVE
TEST CASES

This section will outline the test cases investigated in this work. Three problems will be analysed involving a liquid column in a horizontal duct of rectangular section. The viscous, incompressible fluid is initially at rest. Under the force of gravity, the column begins to collapse. The collapse will generate a hydraulic bore that will impact a structure downstream. The test cases are as follows: (1) water column of varying initial heights, (2) structure of varying heights and (3) structure of varying lengths.

The dam break problem was investigated experimentally by Zhou et al (1999). The setup includes a water column of height 0.6 m, length 1.2 m and width 1 m and a tank of height 2.0 m, length 3.22 m and width 1 m (see Figure 2). Subsequently, the configuration was used for numerical investigations by Nielsen (2003), Abdolmaleki et al. (2004) and Ji et al. (2013). These works use the tanks right wall, located at x = 3.22 m, for readings. However, the inclusion of a structure in the present work, would limit the downstream length available for bore formation. It is for this reason, the length of the tank will be extended to 4.32 m and the structures left face placed at x = 3.22 m. Configuration and variables of individual problems will be stated throughout this section.

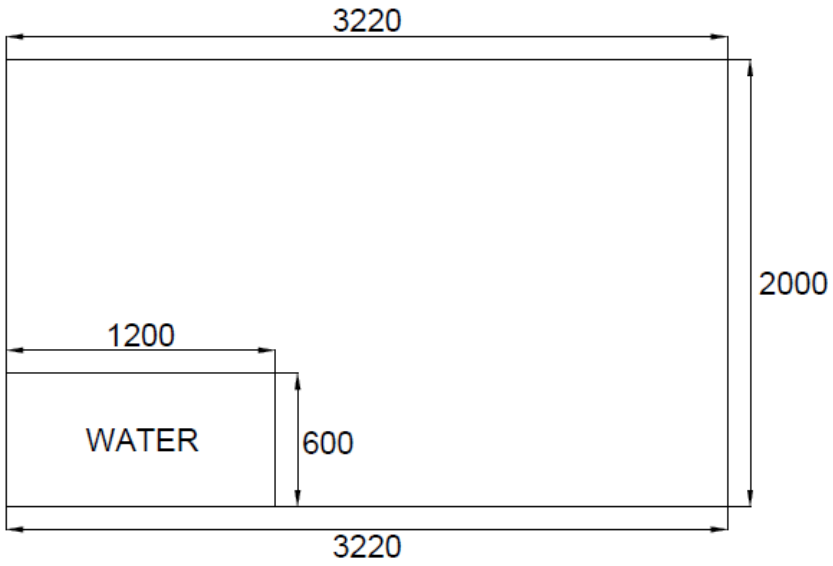

Figure 2: The configuration used by Zhou et al. (1999) to investigate forces of a dam-break induced bore on a vertical wall

5.1 Test Case 1 – Dam height

The first test problem will investigate the effect of water column height on the peak impact force induced on a structure. A water column will collapse in a horizontal duct of rectangular cross section and impact a structure located downstream. The rectangular column of a viscous, incompressible fluid is initially at rest. Due to the force of gravity, the column will start to collapse.

Table 7 summarises the initial water column heights investigated in this problem. The model represents a channel of length 4.32 m, height 2 m, and width 1 m. The water column of varying height H, length 1.2 m and width 1 m is positioned in the lower left corner. The structure of height 0.3 m, length 0.1 m and width 1 m is located at x = 3.22 m. Figure 3 shows the configuration of the problem. The force of fluid flow on the structure is measured in relation to the lower left corner of the structure (x = 3.22 m, y = 0.0 m).

Table 7: The variables considered in computations of a dam-break induced bore on a vertical structure, with a dam of varying height

Case	**Water column height H (m)**
1	0.30
2	0.60
3	0.90
4	1.20
5	1.50
6	1.80

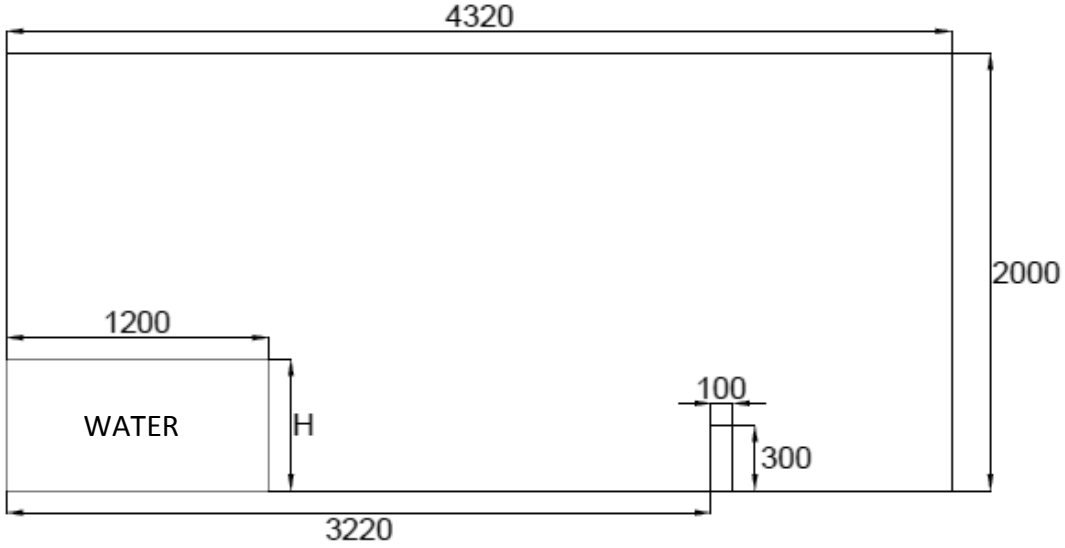

Figure 3: The configuration used in computations of a dam-break induced bore on a vertical structure, with a dam of varying height (mm)

5.2 Test Case 2 – Structure height

The second test problem will investigate the effect of structure height on the force induced by a hydraulic bore. The nature of the experiment is as in Section 5.1; a water column will collapse under the force of gravity and impact a structure downstream.

The problem variables are summarised in Table 8. The configuration is shown in Figure 4. The reservoir will remain unchanged. Whereas, the water column of height 0.6 m, length 1.2 m and width 1 m will have fixed dimensions. The structure of varying height H, length 0.1 m and width 1 m will vary. The starting position of the water column will be unchanged as will the location of the structure.

Table 8: The variables considered in computations of a dam-break induced bore on a vertical structure of varying height

Case	**Structure height H (m)**
1	0.15
2	0.30
3	0.45
4	0.60
5	0.75

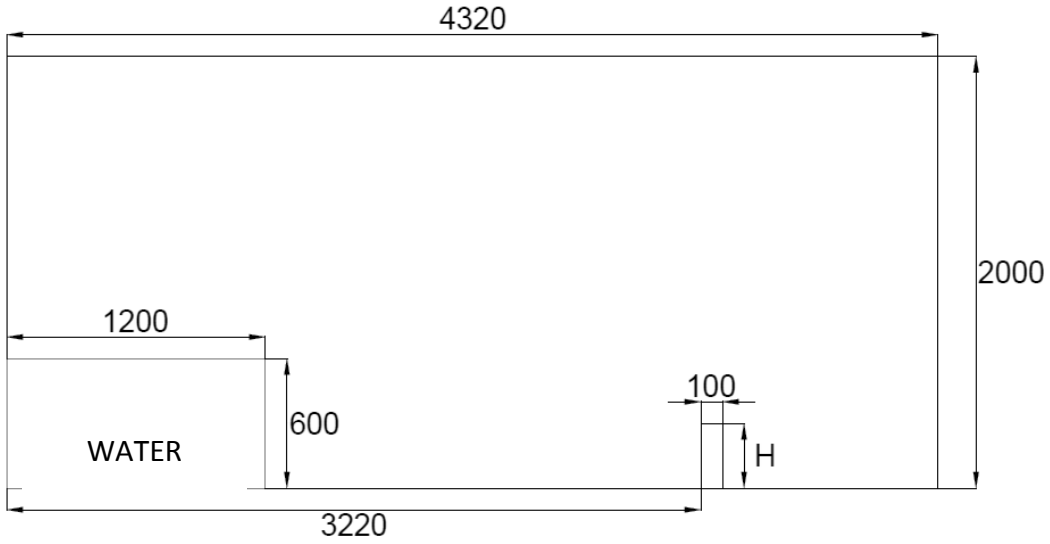

Figure 4: The configuration used in computations of a dam-break induced bore on a vertical structure of varying height (mm)

5.3 Test Case 3 – Structure length

The third test problem will investigate the effect of structure length on the peak impact force induced by a hydraulic bore.

The variables used in this problem are summarised in Table 9. Figure 5 shows the configuration of the problem. The problem will be similar to Test Case 2 described in Section 5.2. A dam of water with fixed dimensions of height 0.6 m, length 1.2 m and width 1 m will collapse under the force of gravity and impact a structure of height 0.3 m, varying length L and width 1 m.

Table 9: The variables considered in computations of a dam-break induced bore on a vertical structure of varying length

Case	Structure length (m)
1	0.05
2	0.10
3	0.15
4	0.20
5	0.25
6	0.30

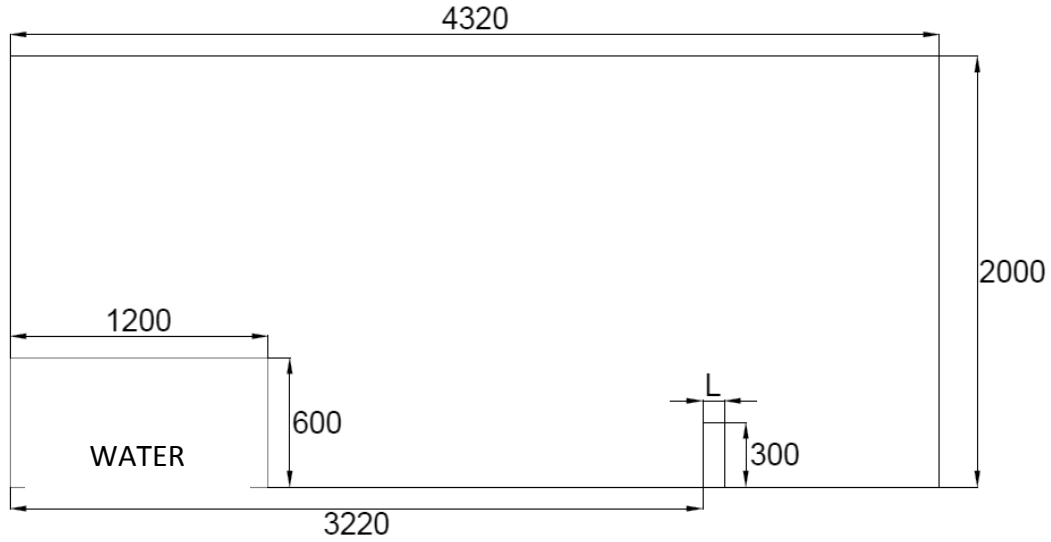

Figure 5: The configuration used in computations of a dam-break induced bore on a vertical structure of varying length (mm)

CHAPTER SIX
RESULTS AND DISCUSSION

Chapter 6 presents the results of three test cases designed to investigate the effects of dam initial height, structure height and structure length on the force imposed by a dam-break induced hydraulic bore.

6.1 Test Case 1 – Dam height

Table 10 shows the numerical results for different initial dam heights. At the moment of time t = 0 s, the water column is released and runs under the gravity force towards the downstream structure. The flow impacts the structure and impinging on it under inertia force, moves upwards. The flow is thinned as it moves up the front face of the structure. When the gravity exceeds the inertia force, the water begins to form a reverse flow moving in the negative x-direction. This formation of a bend in the surface can be seen in Figure 7.

Table 10: Computational results of a dam-break induced bore on a vertical structures, with a dam of varying height

Dam initial height (m)	Peak impact (kN)	Instant of peak impact (s)
0.3	0.51	1.438
0.6	0.87	0.731
0.9	2.37	0.635
1.2	4.37	0.589
1.5	6.34	0.564
1.8	8.01	0.553

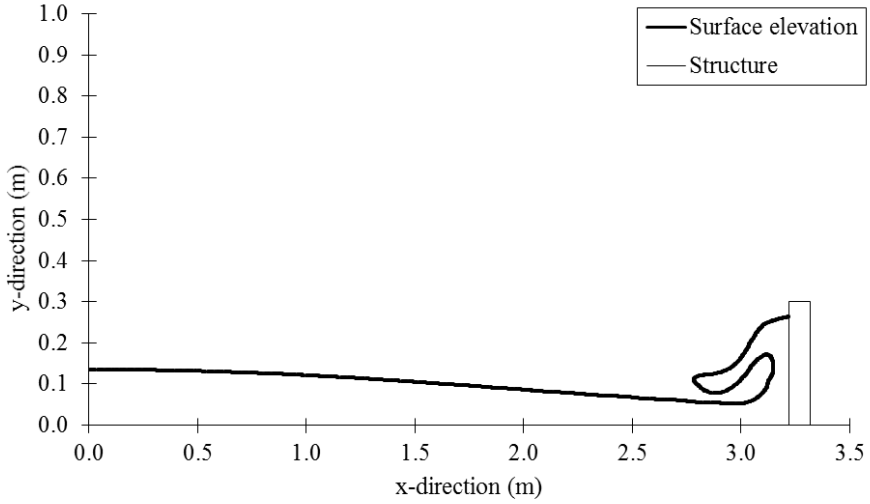

Figure 6: Free surface profile of a dam-break induced bore at moment of peak force for a dam of height 0.3 m

Regarding the case of a dam of initial height 0.3 m, the maximum peak force occurs at the moment of time t = 1.438 s when the reverse flow is fully formed just before it impinges back onto the primary flow, see Figure 7. Regarding cases where the dam initial height is greater than or equal to 0.60 m, the peak force is imposed in the initial impact. The flow profiles are compared for initial dam height greater than or equal to 0.60 m in Figure 8.

Generally, the peak horizontal force increases as the initial dam height increases (Figure 9). This is likely due to bore velocity at the moment of impact. As initial velocity is a result of weight only, it is expected an increase in water mass will produce an increase in velocity. The force-time relationship for a water column of initial height H = 0.3 m shows a very gradual increase of force (Figure 10a). Conversely, for initial column heights greater than or equal to 0.6 m, a large impulse is exerted by the bore on the structure. The force time graphs show similarities in force development (Figure 10b).

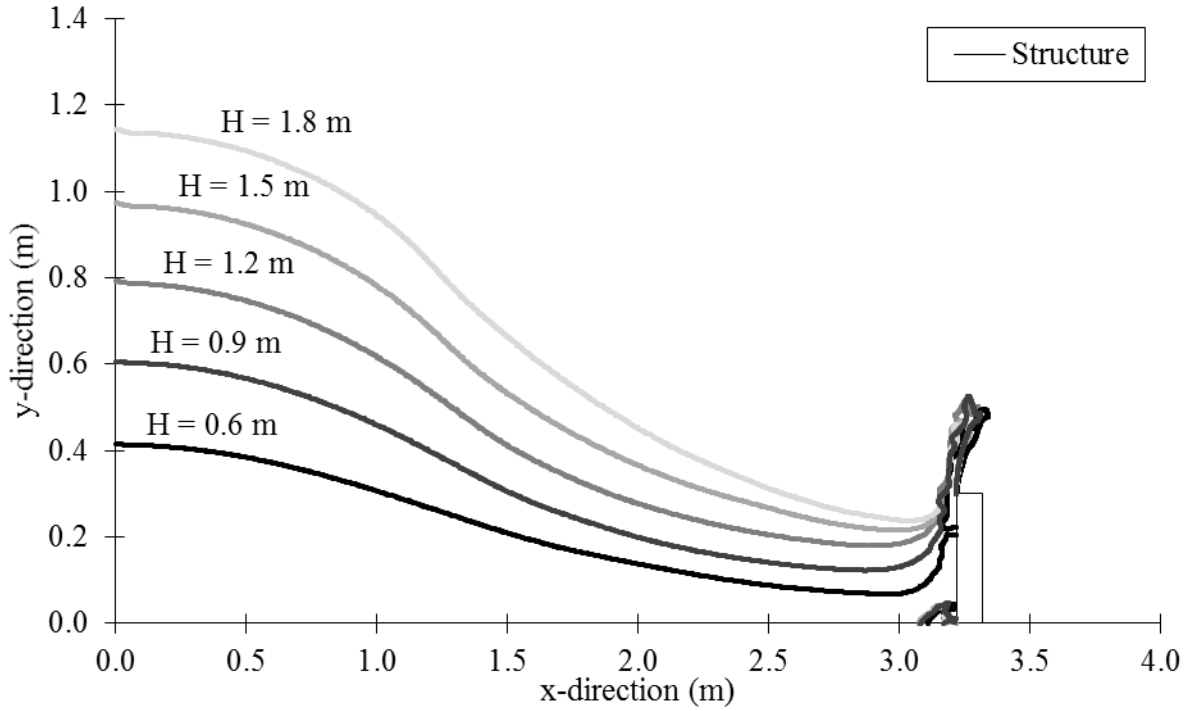

Figure 7: Free surface profile of a dam-break induced bore at moment of peak force for an initial dam height ≥ 0.6 m

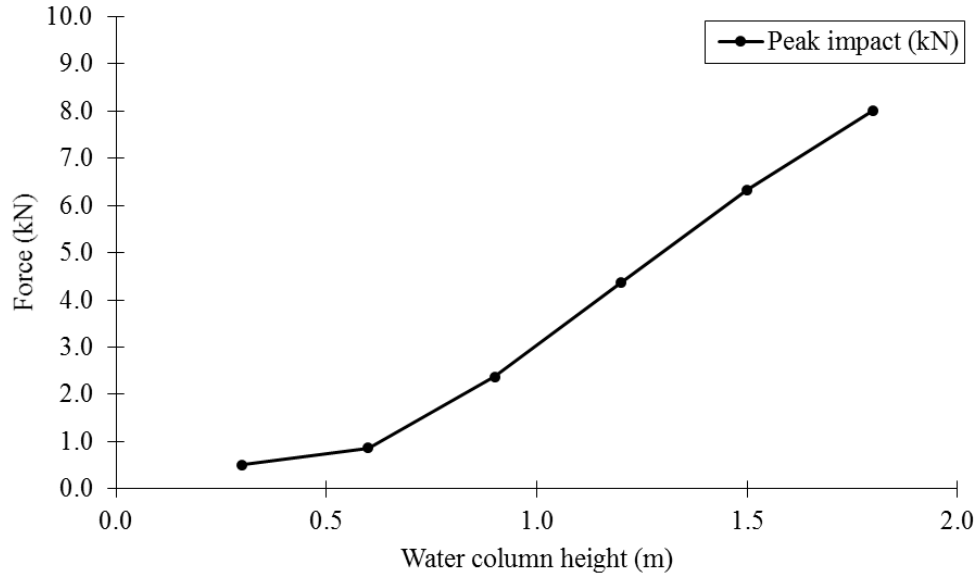

Figure 8: Computational results of peak forces on a vertical structure against initial water column height

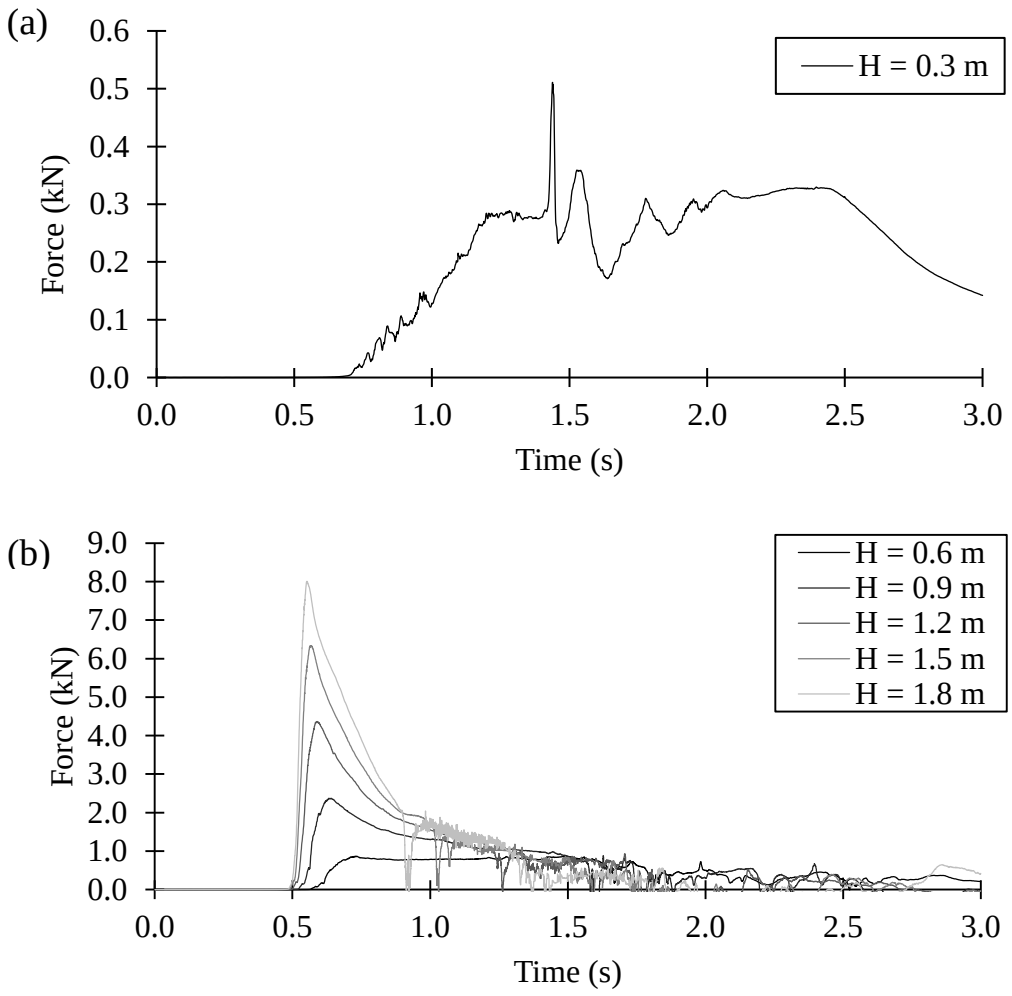

Figure 9: Forces of a bore induced by a dam-break of initial height (a) H =0.3 m and (b) H = 0.6, 0.9, 1.2, 1.5, 1.8 m interacting with a vertical structure

6.2 Test Case 2 – Structure height

Table 11 shows the numerical results for different structure heights. It is evident that peak impact force increases as structure height increases (Figure 11). However, the relationship is non-linear. Analysis of the free surface profile at the instance of peak impact forces shows three very different profiles. Firstly, when the structure height H = 0.15 m and 0.30m, the free surface profile at the peak load shows a thinned layer of runup on the front face of the structure (Figures 12 and 13). Structure heights H = 0.6 m and 0.75 m experiences the peak load after the generation of a reflective wave, just before it impinges back on to the main flow (Figures 14 and 15). Finally, an intermediate profile flow is recorded for structure height H =0.45 m. The intermediate free surface profile at the peak force of a structure with height H = 0.45 m show both a reflective wave that has already impinged on the main flow and a volume of fluid that has passed over the structure (Figure 16).

Table 11: Computational results of a dam-break induced bore on a vertical structure of varying height

Structure height (m)	Peak impact (kN)	Instant of peak impact (s)
0.15	0.70	0.721
0.30	0.87	0.731
0.45	1.18	1.566
0.60	2.12	1.512
0.75	2.52	1.538

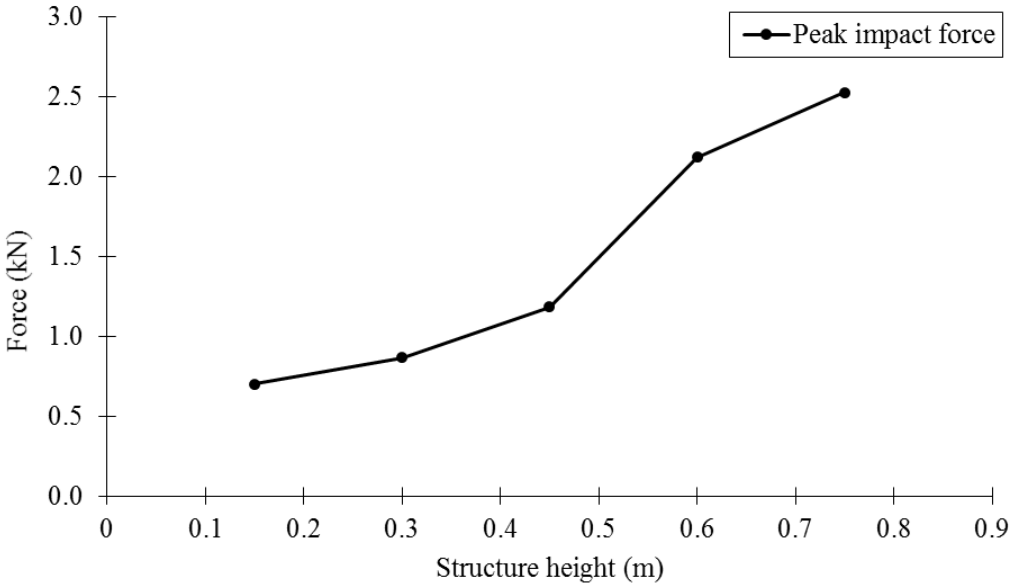

Figure 10: Computational results of peak forces on a vertical structure of varying height

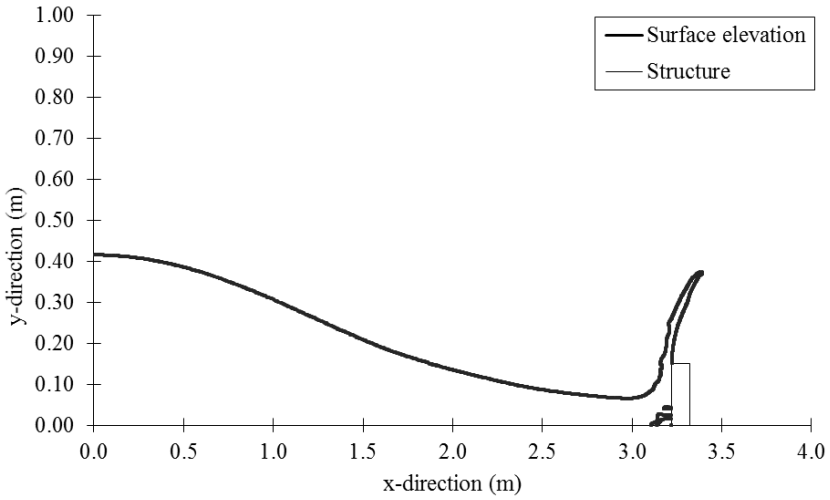

Figure 11: Free surface profile of a dam-break induced bore at moment of peak force for a structure height of 0.15 m

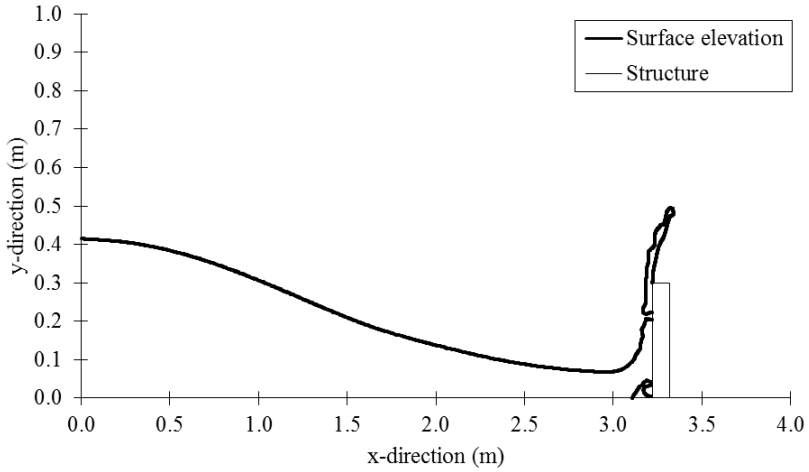

Figure 12: Free surface profile of a dam-break induced bore at moment of peak force for a structure height of 0.3 m

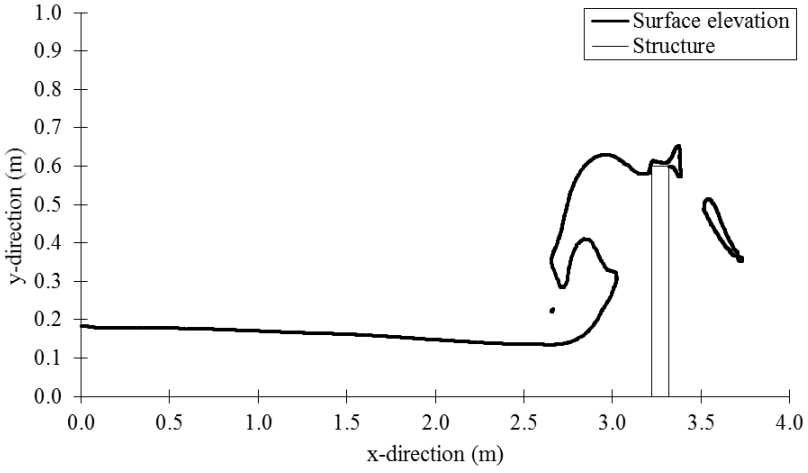

Figure 13: Free surface profile of a dam-break induced bore at moment of peak force for a structure height of 0.6 m

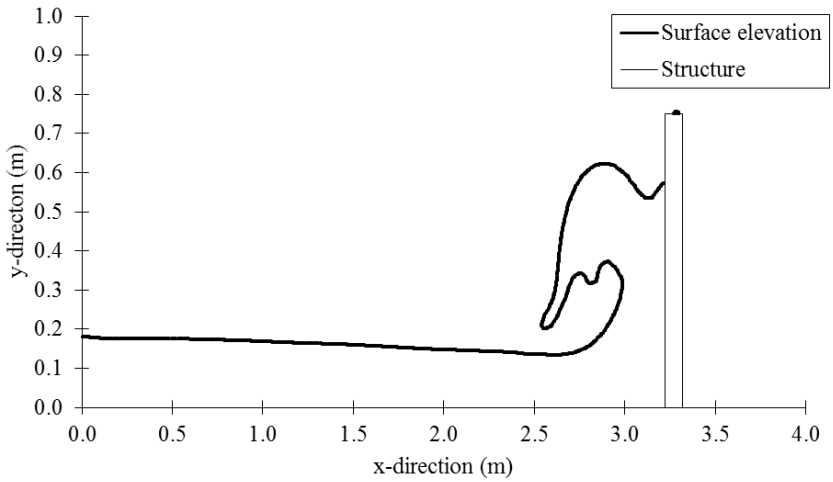

Figure 14: Free surface profile of a dam-break induced bore at moment of peak force for a structure height of 0.75 m

Interestingly, for the case of a structure height of 0.45 m, the peak impact force occurs at a time similar to cases where a rebound wave is generated. However, the magnitude of the peak impact is around the numerical results of a case experiencing peak force during vertical runup on the front face of the structure. It is possible the ratio between the structure height and bore inundation height produced an outcome minimising the peak impact induced by the bore.

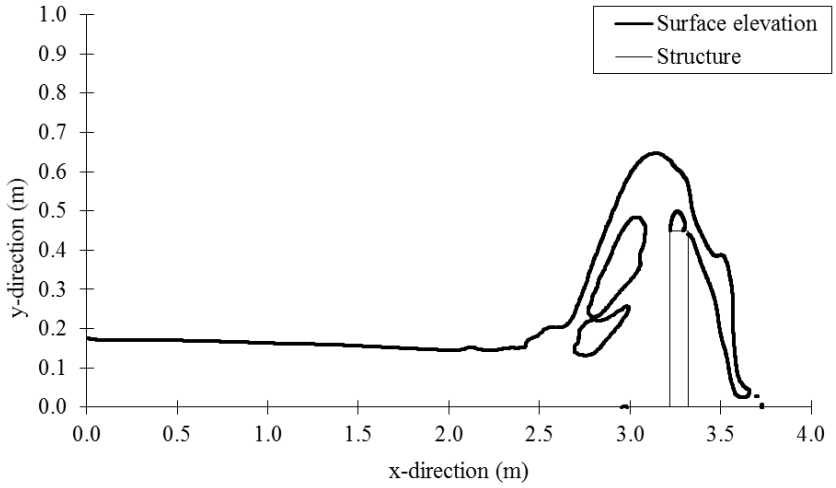

Figure 15: Free surface profile of a dam-break induced bore at moment of peak force for a structure height of 0.45 m

6.3 Test Case 3 – Structure length

Table [CITE] shows the numerical results for different structure lengths. Figure [CITE] shows peak impact force against structure length. At first glance, the magnitude of the peak impact is majorly between 0.85 kN and 0.95 kN. One anomaly result for a structure length of 0.25 m produces a spike in the results, shown in Figure [CITE]. The magnitude of peak force is approximately 1.5 times the remainder of the data. It is likely due to the impingement of a reverse wave on the main flow. When the reverse wave collides with the main flow, the relatively quick displacement of fluid will generate extra velocity moving towards the vertical wall. For this reason, this data point will be ignored for any conclusions made for the effect of structure length.

Table 12: Computational results of a dam-break induced bore on a vertical structure of varying length

Structure length (m)	Peak impact (kN)	Instant of peak impact (s)
0.05	0.95	1.554
0.10	0.87	0.731
0.15	0.87	0.734
0.20	0.87	0.731
0.25	1.30	1.711
0.30	0.86	0.726

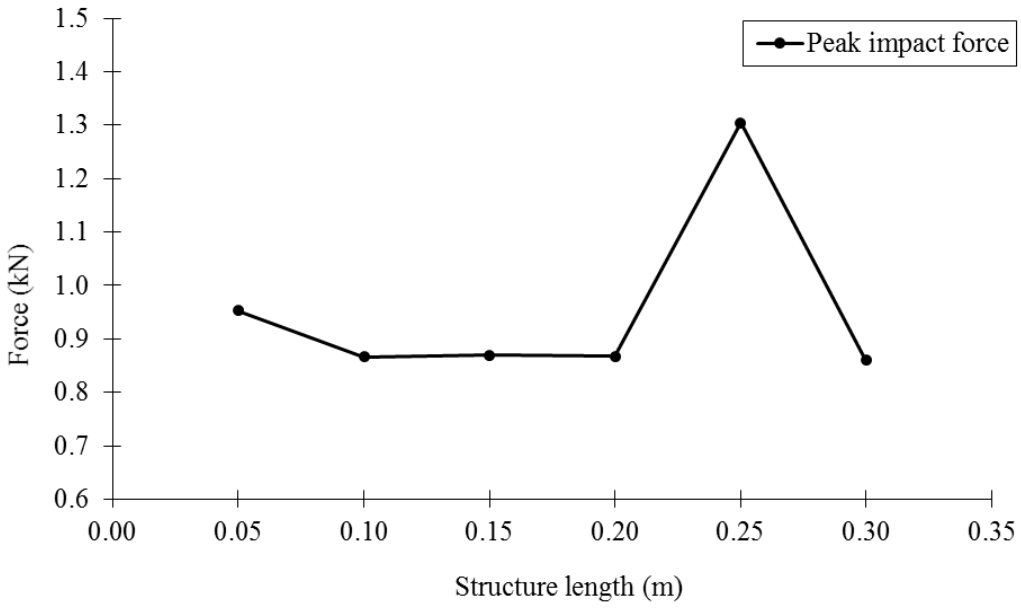

Figure 16: Computational results of peak forces on a vertical structure of varying length

At the initial time t = 0 s, the water column begins to collapse under the force of gravity. The flow moves towards the structure forming a bore. Regarding cases of structure length 0.10 m, 0.15 m, 0.20 m and 0.30 m, at the moment of time t ≈ 0.73 s a thin layer of fluid runup is observed on the front face of the structure and the peak impact force is exerted (Figures [CITE]). The peak impact appears to be limited at approximately 0.87 kN.

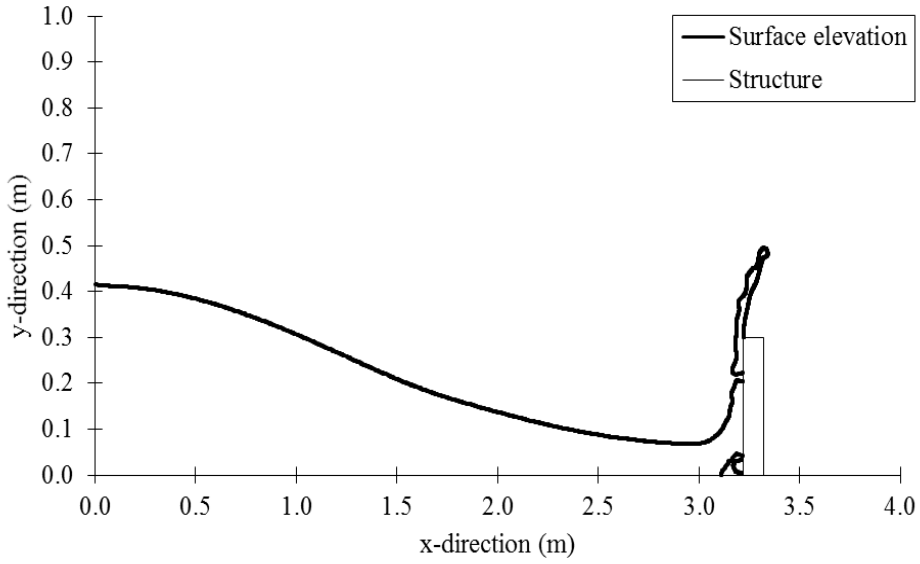

Figure 17: Free surface profile of a dam-break induced bore at moment of peak force for a structure length of 0.10 m

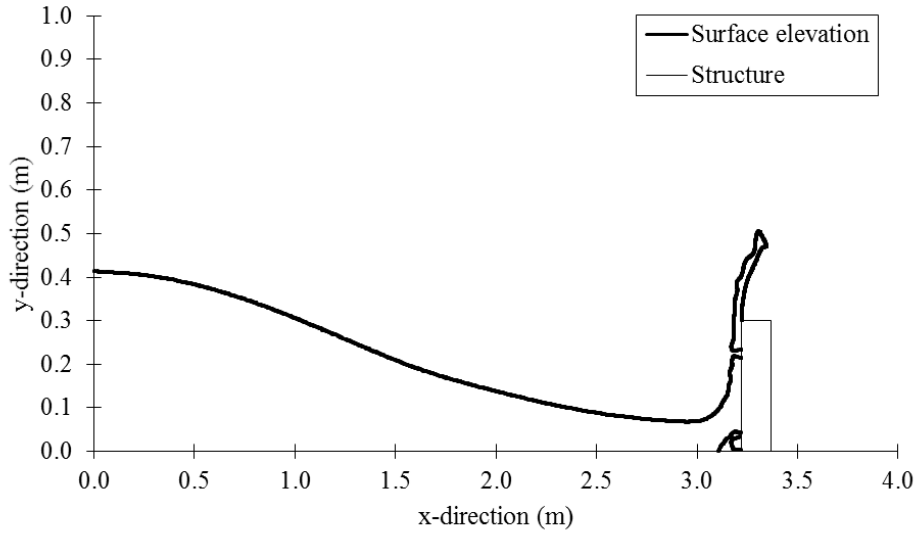

Figure 18: Free surface profile of a dam-break induced bore at moment of peak force for a structure length of 0.15 m

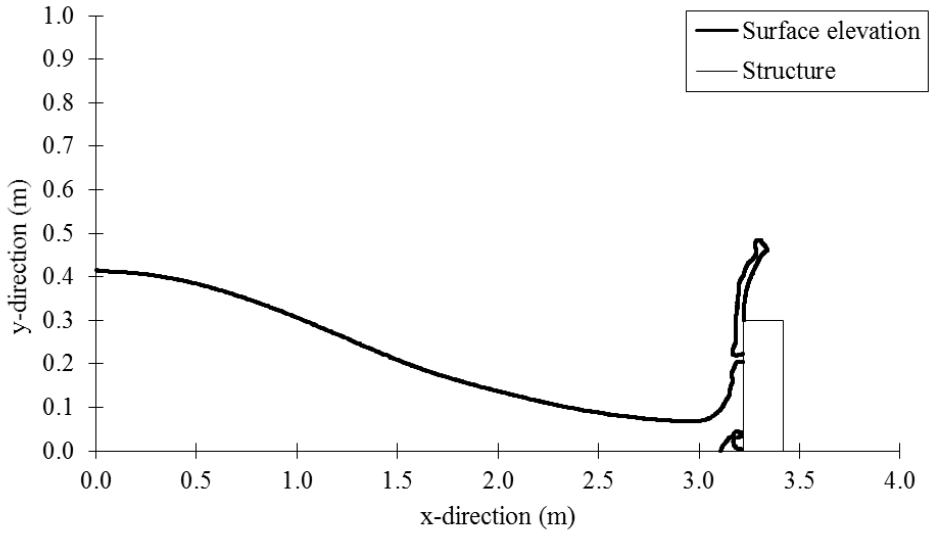

Figure 19: Free surface profile of a dam-break induced bore at moment of peak force for a structure length of 0.20 m

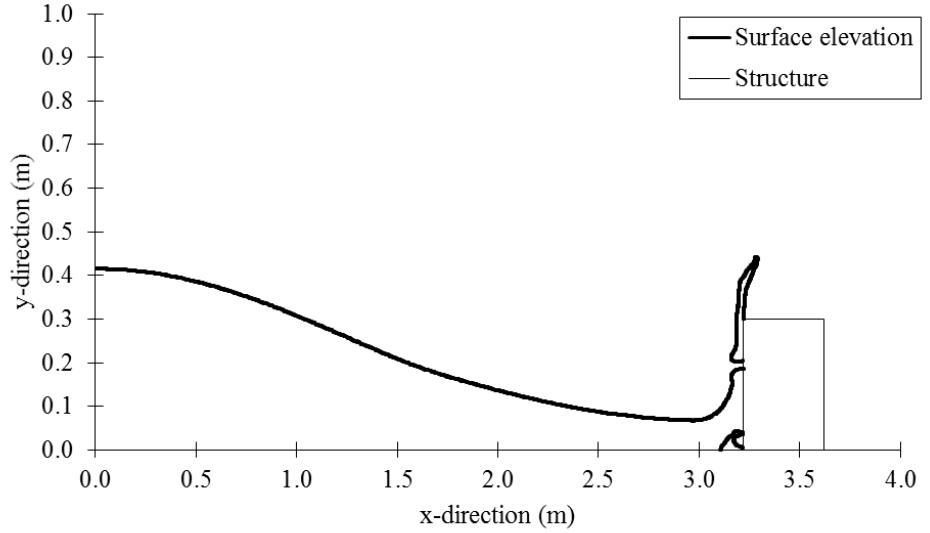

Figure 20: Free surface profile of a dam-break induced bore at moment of peak force for a structure length of 0.30 m

For a structure length of 0.05 m, the peak impact force is comparable those experienced in structures of length 0.10 m, 0.15 m, 0.20 m and 0.30 m. Despite the time of this impact and free surface profile shows similarities with a structure of length 0.25 m. The flow profiles show a large body of water passing over the structure and the main body almost horizontal and settled. Hydrostatic forces may be significantly higher in these cases than those with a smaller peak force.

Overall, structure length appears to have no effect on the forces exerted on that structure by a hydraulic bore. However, if the case was such that overflowing fluid collided with the top of the structure, i.e. the case of a coastal deck, the structure may experience large vertical forces

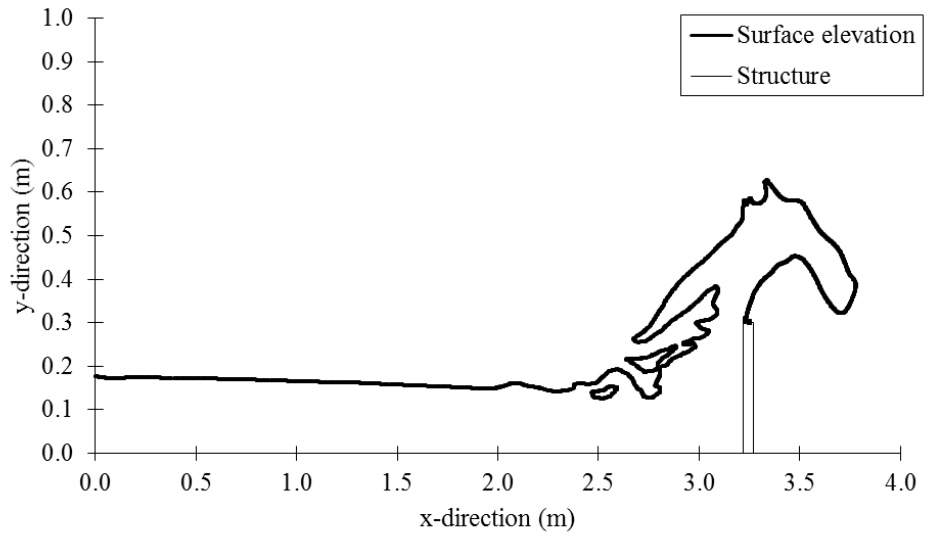

Figure 21: Free surface profile of a dam-break induced bore at moment of peak force for a structure length of 0.05 m

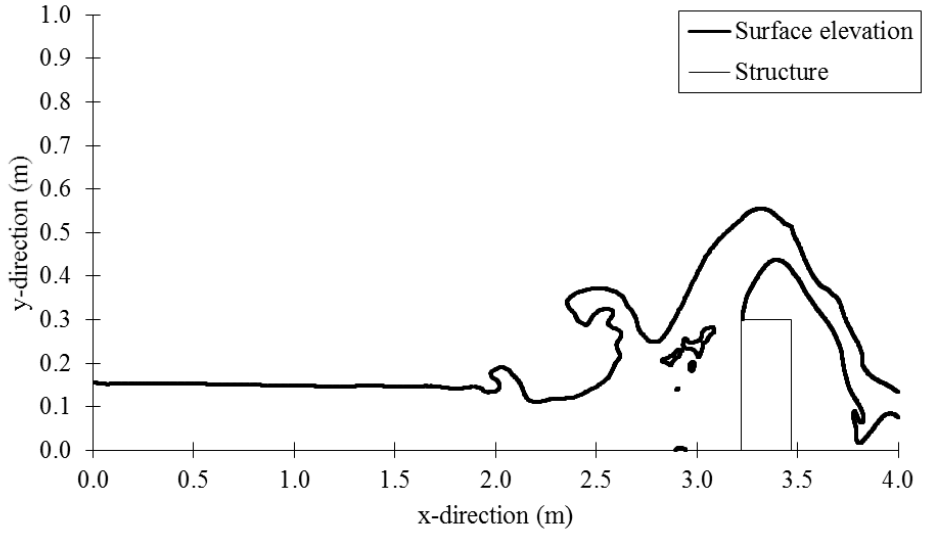

Figure 22: Free surface profile of a dam-break induced bore at moment of peak force for a structure length of 0.25 m

6.4 Summary

The force exerted on a structure by a hydraulic bore generated by simulation of a dam-break was investigated for three test cases: dam-initial height, structure height and structure length.

The first problem considered six initial heights of the water column simulating a dam. The velocity of the fluid is dependent on gravity. Therefore, by increasing the height (thus, weight) of the water column, the velocity will increase. Results showed peak force exerted on the structure increase as the initial dam height was increased. The force-time relationship of bore-structure interaction was analysed. Despite the difference in magnitude, the force-time graphs showed similarities in shape for dams of initial height greater than or equal to 0.6 m. This suggests that further enlargement of initial dam height would exert a greater force on the structure, in a similar manner to those examined in the present work.

The second problem considered five heights of the downstream structure. The force exerted on the structure is observed to increase as the structure height increases. This suggests tall support structures are more at risk of experiencing large lateral forces than short structures. Smaller structure heights allow some fluid to pass over the structure, avoiding some hydrodynamic force. When the structure height is approximately equal to the maximum runup height of the hydraulic bore it is expected that peak force will level out.

The final problem considered six lengths of the downstream structure. The length on the structure was shown to have little to no effect on the force exerted on the structure, disregarding the anomaly result.

CHAPTER SEVEN
CONCLUSION

This thesis has highlighted the requirement for the investigation of dam-break flows. A review of existing literature was carried out to gain an in-depth understanding of hydraulic bore behaviour and their interaction with structures. The details of previous analytical, experimental and numerical investigations proved useful in learning about dam-break flow. Further, common methods of approach to dam-break problems were identified.

Numerical modelling of a dam-break simulation held advantages over analytical and experimental methods. The OpenFOAM solver interFoam was used to solve the Navier-Stokes equations to investigate the effects of initial dam height, structure height and structure length on the lateral forces imposed on a structure downstream. The results in this work can be used for comparable methods with future analytical and laboratory experiments.

From the analysis of CFD computations the following conclusions were made:

- Regarding initial dam height, the peak lateral force exerted on a vertical structure increases as the initial dam height increases. Increase in dam height increases impact velocity of flow. Force-time relationships display similar shapes when peak force occurs during structure run up, increasing in magnitude as bore volume and velocity increase.

- Regarding structure height, the peak lateral force exerted on a vertical structure increases as the structure height increases. The peak force will also relate to the maximum runup height of the bore on the structure. At the point where structure height is greater than the maximum runup height of the bore, addition structure height will not affect the peak force.

- The length of a vertical coastal structure appears to have no correlation to the peak lateral force. However, the presence of a coastal deck would likely experience large vertical forces imposed from overflow.

7.1 Further Work

Based on the results from this thesis, there are some recommendations that would assist future research in developing an understanding of dam-break induced hydraulic bore interaction with a vertical structure. The recommendations are as follows:

- Parameters that were unable to be studied in this thesis include the effect of subsequent structures. Many coastal structures involve subsequent vertical supports, e.g. bridges, therefore the analysis of subsequent structures of the same height are of key importance to the understanding of how such structures will be affected by a hydraulic bore. Regarding subsequent structures of increasing or decreasing height, implications of breaker walls could be analysed as a preventative measure to dam-break flows.
- Only lateral forces were considered in this work. Other forces such as vertical or moment around a set axis may be worth investigating.
- Debris force is acknowledged to play a big role in the lateral forces experience on a vertical structure by a hydraulic bore. If possible, future work should incorporate the effect of debris forces on the initial impact of a hydraulic bore.

References

Abdolmaleki, K., Thiagarajan, K. P. & Morris-Thomas, M. T., 2004. Simulation of the dam break problem and impact flows using a Navier-Stokes solver. *Simulation,* Volume 13, p. 17.

Bellos, C. V. & Sakkas, J. G., 1987. 1-D dam-break flood-wave propagation on dry bed. *Journal of Hydraulic Engineering,* 113(12), pp. 1510-1524.

Bell, S. W., Elliot, R. C. & Hanif Chaudhry, M., 1992. Experimental results of two-dimensional dam-break flows. *Journal of Hydraulic Research,* 30(2), pp. 225-252.

Biscarini, C., Francesco, S. D. & Manciola, P., 2010. CFD modelling approach for dam break flow studies. *Hydrology and Earth System Sciences,* Volume 14, pp. 705-718.

Chanson, H., 2006. Tsunami Surges on Dry Coastal Plains: Application of Dam Break Wave Equations. *Coastal Engineering Journal,* 48(4), pp. 355-370.

Choi, B. H., Hong, S. J. & Pelinovsky, E., 2006. Distribution of runup heights of the December 26, 2004 tsunami in the Indian Ocean. *Geophysical research letters,* 33(13).

Colicchio, G., Colagrossi, A., Greco, M. & Landrini, M., 2002. Free-surface flow after a dam break: a comparative study. *Ship Technol. Res,* 49(3), pp. 95-104.

Cross, R. H., 1967. Tsunami surge forces. *Journal of the Waterways and Harbors Division,* 93(4), pp. 201-234.

Cumberbatch, E., 1960. The impact of a water wedge on a wall. *Journal of Fluid Mechanics,* 7(3), pp. 353-374.

Dressler, R. F., 1952. Hydraulic resistance effect upon the dambreak functions. *J Res Natl Bureau Stand,* 49(3), pp. 217-225.

Dressler, R. F., 1954. Comparison of theories and experiments for the hydraulic dam-break wave. *Int. Assoc. Sci. Hydrology,* 3(38), pp. 319-328.

Eaket, J., Hicks, F. E. & Peterson, A. E., 2005. Use of stereoscopy for dam break flow measurement. *Journal of Hydraulic Engineering,* 131(1), pp. 24-29.

Fennema, R. J. & Chaudhry, M. H., 1987. Simulation of one-dimensional dam-break flows. *Journal of Hydraulic Research,* 25(1), pp. 41-51.

Fraccarollo, L. & Toro, E. F., 1995. Experimental and numerical assessment of the shallow water model for two-dimensional dam-break type problems. *Journal of Hydraulic Research,* 33(6), pp. 843-864.

Frazão, S. S. & Zech, Y., 2002. Dam break in channels with 90 bend. *Journal of Hydraulic Engineering,* 128(11), pp. 956-968.

Frazão, S. S. & Zech, Y., 2007. Experimental study of dam-break flow against an isolated obstacle. *Journal of Hydraulic Research,* 45(1), pp. 27-36.

Gingold, R. A. & Monaghan, J. J., 1977. Smoothed particle hydrodynamics: theory and application to non-spherical stars. *Monthly notices of the royal astronomical society,* 181(3), pp. 375-389.

Gómez-Gesteira, M., Cerqueiro, D., Crespo, C. & Dalrymple, R. A., 2005. Green water overtopping analyzed with a SPH model. *Ocean Engineering,* 32(2), pp. 223-238.

Gómez-Gesteira, M. & Dalrymple, R. A., 2004. Using a three-dimensional smoothed particle hydrodynamics method for wave impact on a tall structure. *Journal of Waterway, Port, Coastal, and Ocean Engineering,* 130(2), pp. 63-69.

Hervouet, J.-M. & Petitjean, A., 1999. Malpasset dam-break revisited with two-dimensional computations. *Journal of Hydraulic Research,* 37(6), pp. 777-788.

Hirt, C. W. & Nichols, B. D., 1981. Volume of Fluid (VOF) Method for the Dynamics of Free Boundaries. *Journal of Computational Physics,* Volume 39, pp. 201-225.

Janosi, I. M., Jan, D., Szabó, K. G. & Tél, T., 2004. Turbulent drag reduction in dam-break flows. *Experiments in Fluids,* 37(2), pp. 219-229.

Ji, Q., Zhao, X. & Dong, S., 2013. Numerical Study of Violent Impact Flow Using a CIP-Based Model. *Journal of Applied Mathematics,* Volume 2013.

Kulikov, E. A., Rabinovich, A. B. & Thomson, R. E., 2005. Estimation of tsunami risk for the Coasts of Peru and Northern Chile. *Natural Hazards,* 35(2), pp. 185-209.

Kundu, P. K. & Cohen, I. M., 2008. *Fluid mechanics.* 4th ed. Amsterdam: Boston: Academic Press.

LaRocque, L. A., Imran, J. & Hanif Chaudhry, M., 2013. Experimental and Numerical Investigations of Two-Dimensional Dam-Break Flows. *Journal of Hydraulic Engineering,* 139(6), pp. 569-579.

Lavigne, F. et al., 2007. Field observations of the 17 July 2006 Tsunami in Java. *Natural Hazards and Earth System Science,* 7(1), pp. 177-183.

Miller, S. & Hanif Chaudhry, M., 1989. Dam-break flows in curved channel. *Journal of Hydraulic Engineering,* 115(11), pp. 1465-1478.

Monaghan, J. J. & Kos, A., 1999. Solitary waves on a Cretan beach. *Journal of Waterway, Port, Coastal, and Ocean Engineering,* 125(3), pp. 145-155.

Nielsen, K. B., 2003. Numerical Prediction of Green Water Loads on Ships.

Nistor, I. et al., 2010. Tsunami-Induced Forces on Structures. *Handbook of Coastal and Ocean Engineering,* pp. 261-286.

Nouri, Y., Nistor, I., Palermo, D. & Cornett, A., 2010. Experimental investigation of tsunami impact on free standing strucutres. *Coastal Engineering Journal,* 52(01), pp. 43-70.

Okal, E. A. et al., 2010. Field Survery of the Samoa Tsunami of 29 September 2009. *Seismological Research Letters,* 81(4), pp. 577-591.

Palermo, D., Nistor, I., Nouri, Y. & Cornett, A., 2009. Tsunami loading of near-shoreline structures: a primer. *Canadian Journal of Civil Engineering,* 36(11), pp. 1804-1815.

Ramsden, J. D., 1993. Tsunamis: forces on a vertical wall caused by long waves, bores, and surges on a dry bed.

Ramsden, J. D., 1996. Forces on a vertical wall due to long waves, bores, and dry-bed surges. *Journal of Waterway, Port, Coastal, and Ocean Engineering,* 122(3), pp. 134-141.

Ramsden, J. D. & Raichlen, F., 1990. Forces on vertical wall caused by incident boers. *Journal of Waterwat, Port, Coastal, and Ocean Engineering,* 116(5), pp. 592-613.

Ritter, A., 1892. Die Fortpflanzung von Wasserwellen. *Zeitschrift Verein Deutscher Ingenieure,* 36(2), pp. 947-954.

Robertson, I. N., Paczkowski, K., Riggs, H. R. & Mohamed, A., 2013. Experimental investigation of tsunami bore forces on vertical walls. *Journal of Offshore Mechanics and Arctic Engineering,* 135(2), p. 021601.

Si, Y., 1998. *The world's most catastrophic dam failures.* s.l.:Qing (1998a).

Snodgrass, F. E., Rice, E. K. & Hall, M., 1951. University of California, Berkeley, CA. *Inst. of Engineering Research,* Technical Report Series 35(4).

Stansby, P. K., Chegini, A. & Barnes, T. C. D., 1998. The initial stages of dam-break flow. *Journal of Fluid Mechanics,* Volume 374, pp. 407-424.

Stoker, J. J., 1957. *Waler Waves: The mathematical Theory with Applications.* s.l.:Intersciences.

Valiana, A., Caleffi, V. & Zanni, A., 2002. Case study: Malpasset dam-break simulation using a two-dimensional finite volume method. *Journal of Hydraulic Engineering,* 128(5), pp. 460-472.

Wang, J. S., Ni, H. G. & He, Y. S., 2000. Finite-difference TVD scheme for computation of dam-break problems. *Journal of Hydraulic Engineering,* 126(4), pp. 253-262.

Wang, X. & Liu, P. L.-F., 2006. An analysis of 2004 Sumatra earthquake fault plane mechanisms and Indian Ocean tsunami. *Journal of Hydraulic Research,* 44(2), pp. 147-154.

Whitham, G. B., 1955. The effects of hydraulic resistance in the dam-break problem. *Proc R Soc Lond,* 227(Serie A), pp. 399-407.

Yeh, H., 2006. Maximum Fluid Forces in the Tsunami Runup Zone. *Journal of Waterway, Port, Coastal, and Ocean Engineering,* 132(6), pp. 496-500.

Yeh, H. H. J., Robertson, I. & Preuss, J., 2005. *Development of design guidelines for structures that serve as tsunami vertical evacuation sites.* (Vol. 4) ed. s.l.:Washington State Department of Natural Resources, Division of Geology and Earth Resources.

Yue, W., Lin, C.-L. & Patel, V. C., 2003. Numerical simulation of unsteady multidimensional free surface motions by level set method. *International Journal for Numerical Methods in Fluids,* Volume 42, pp. 853-884.

Zhainakov, A. Z. & Kurbanaliev, A. Y., 2013. Verification of the open package OpenFOAM on dam break problems. *Thermophysics and Aeromechanics*, 20(4), pp. 451-461.

Zhou, Z. Q., Kat, J. O. D. & Buchner, B., 1999. *A nonlinear 3-D approach to simulate green water dynamics on deck.* Nantes, 7th Intl. Conf. Num. Ship Hydrodynamics.

Appendix

A – Model

Constant directory

g file

```
FoamFile
{
    version     2.0;
    format      ascii;
    class       uniformDimensionedVectorField;
    location    "constant";
    object      g;
}
// * * * * * * * * * * * * * * * * * * * * * * * * * * * * * * * * * * * * * * * * * * * * //

dimensions      [0 1 -2 0 0 0 0];
value           (0 -9.81 0);

// ************************************************************************* //
```

transportProperties file

```
FoamFile
{
    version     2.0;
    format      ascii;
    class       dictionary;
    location    "constant";
    object      transportProperties;
}
// * * * * * * * * * * * * * * * * * * * * * * * * * * * * * * * * * * * * * * * * * * * * //

phases (water air);

water
{
    transportModel  Newtonian;
    nu              1e-06;
    rho             1000;
}

air
{
    transportModel  Newtonian;
    nu              1.48e-05;
    rho             1.225;
}

sigma            0.07;

// ************************************************************************* //
```

turbulenceProperties file

```
FoamFile
{
    version     2.0;
    format      ascii;
    class       dictionary;
    location    "constant";
    object      turbulenceProperties;
}
// * * * * * * * * * * * * * * * * * * * * * * * * * * * * * * * * * * * * * * * * * * * * * * * * * * * * * * * * //

simulationType  laminar;

// ************************************************************************* //
```

System directory

blockMesh file example (subsequent structures)

controlDict file

```
FoamFile
{
    version     2.0;
    format      ascii;
    class       dictionary;
    location    "system";
    object      controlDict;
}
// * * * * * * * * * * * * * * * * * * * * * * * * * * * * * * * * * * * * * * * * * * * * //

application     interFoam;
startFrom       startTime;
startTime       0;
stopAt          endTime;
endTime         3;
deltaT          0.001;
writeControl    adjustableRunTime;
writeInterval   0.1;
purgeWrite      0;
writeFormat     ascii;
writePrecision  4;
writeCompression uncompressed;
timeFormat      general;
timePrecision   4;
runTimeModifiable yes;
adjustTimeStep  yes;
maxCo           1;
maxAlphaCo      1;
maxDeltaT       1;

functions
{
        #include "forces"
        #include "freeSurface"
}
```

```
forces
{
        type                    forces;
        libs                    ("libforces.so");
        patches                 (object);
        writeControl            timeStep;
        writeInterval           1;
        CofR                    (3.22 0 0);
        pName                   p_rgh;
        UName                   U;
        rhoName                 rhoInf
        rhoInf                  1000;
        log                     on;
        dragDir                 (1 0 0);
        liftDir                 (0 1 0);
        pitchAxis               (0 0 1);
}


freeSurface
        {
        type                    surfaces;
        libs                    ("libsampling.so");
        outputControl           timeStep;
        outputInterval          1;
        surfaceFormat           raw;
        fields                  (alpha.water);
        surfaces                (
                                freeSurface
                                        {
                                                type            isoSurfaceCell;
                                                isoField        alpha.water;
                                                isoValue        0.5;
                                                interpolate     false;
                                                regularise      false;
                                        }
                                );
        interpolationScheme     cell;
        }
```

fvSchemes file

```
FoamFile
{
    version     2.0;
    format      ascii;
    class       dictionary;
    location    "system";
    object      fvSchemes;
}
// * * * * * * * * * * * * * * * * * * * * * * * * * * * * * * * * * * * * * * * * * * * * //

ddtSchemes
{
    default         Euler;
}

gradSchemes
{
    default         Gauss linear;
}

divSchemes
{
    div(rhoPhi,U)  Gauss linearUpwind grad(U);
    div(phi,alpha)  Gauss vanLeer;
    div(phirb,alpha) Gauss linear;
    div(((rho*nuEff)*dev2(T(grad(U))))) Gauss linear;
}

laplacianSchemes
{
    default         Gauss linear corrected;
}

interpolationSchemes
{
    default         linear;
}

snGradSchemes
{
    default         corrected;
}

// ************************************************************************* //
```

fvSolution file

```
FoamFile
{
    version     2.0;
    format      ascii;
    class       dictionary;
    location    "system";
    object      fvSolution;
}
// * * * * * * * * * * * * * * * * * * * * * * * * * * * * * * * * * * * * * * * * * * * * //

solvers
{
    "alpha.water.*"
    {
        nAlphaCorr      2;
        nAlphaSubCycles 1;
        cAlpha          1;

        MULESCorr       yes;
        nLimiterIter    5;

        solver          smoothSolver;
        smoother        symGaussSeidel;
        tolerance       1e-8;
        relTol          0;
    }

    "pcorr.*"
    {
        solver          PCG;
        preconditioner  DIC;
        tolerance       1e-5;
        relTol          0;
    }

    p_rgh
    {
        solver          PCG;
        preconditioner  DIC;
        tolerance       1e-05;
        relTol          0.05;
    }
```

```
    p_rghFinal
    {
        $p_rgh;
        relTol          0;
    }

    U
    {
        solver          smoothSolver;
        smoother        symGaussSeidel;
        tolerance       1e-05;
        relTol          0;
    }
}

PIMPLE
{
    momentumPredictor   no;
    nOuterCorrectors    1;
    nCorrectors         3;
    nNonOrthogonalCorrectors 0;
}

relaxationFactors
{
    equations
    {
        ".*" 1;
    }
}
```

Time directory

alpha.water file

```
FoamFile
{
    version     2.0;
    format      ascii;
    class       volScalarField;
    object      alpha.water;
}
// * * * * * * * * * * * * * * * * * * * * * * * * * * * * * * * * * * * * * * * * * * * * //

dimensions      [0 0 0 0 0 0 0];

internalField   uniform 0;

boundaryField
{
    leftWall
    {
        type            zeroGradient;
    }
    rightWall
    {
        type            zeroGradient;
    }
    lowerWall
    {
        type            zeroGradient;
    }
    object
    {
        type            zeroGradient;
    }
    atmosphere
    {
        type            inletOutlet;
        inletValue      uniform 0;
        value           uniform 0;
    }
    defaultFaces
    {
        type            empty;
    }
}
```

p_rgh file

```
FoamFile
{
    version     2.0;
    format      ascii;
    class       volScalarField;
    object      p_rgh;
}
// * * * * * * * * * * * * * * * * * * * * * * * * * * * * * * * * * * * * * * * * * * * * //

dimensions      [1 -1 -2 0 0 0 0];

internalField   uniform 0;

boundaryField
{
    leftWall
    {
        type            fixedFluxPressure;
        value           uniform 0;
    }
    rightWall
    {
        type            fixedFluxPressure;
        value           uniform 0;
    }
    lowerWall
    {
        type            fixedFluxPressure;
        value           uniform 0;
    }
    object
    {
        type            zeroGradient;
        value           uniform 0;
    }
    atmosphere
    {
        type            totalPressure;
        p0              uniform 0;
    }
    defaultFaces
    {
        type            empty;
    }
}
```

U file

```
FoamFile
{
    version     2.0;
    format      ascii;
    class       volVectorField;
    location    "0";
    object      U;
}
// * * * * * * * * * * * * * * * * * * * * * * * * * * * * * * * * * * * * * * * * * * * * //

dimensions      [0 1 -1 0 0 0 0];

internalField   uniform (0 0 0);

boundaryField
{
    leftWall
    {
        type            noSlip;
    }
    rightWall
    {
        type            noSlip;
    }
    lowerWall
    {
        type            noSlip;
    }
    object
    {
      type              noSlip;
    }
    atmosphere
    {
        type            pressureInletOutletVelocity;
        value           uniform (0 0 0);
    }
    defaultFaces
    {
        type            empty;
    }
}
```

Appendix

B – Organisation of results

Python code

Forces data to dictionaries

```
#!/usr/bin/python

import os

os.chdir('../openfoam/___')
testCaseName = "___"

forces_file = testCaseName+"/postProcessing/forces/0/forces.dat"

def line2dict(line):
    tokens_unprocessed = line.split()
    tokens = [x.replace(")","").replace("(","") for x in tokens_unprocessed]
    floats = [float(x) for x in tokens]
    data_dict = {}
    data_dict['time'] = floats[0]
    force_dict = {}
    force_dict['pressure'] = floats[1:4]
    force_dict['viscous'] = floats[4:7]
    force_dict['porous'] = floats[7:10]
    moment_dict = {}
    moment_dict['pressure'] = floats[10:13]
    moment_dict['viscous'] = floats[13:16]
    moment_dict['porous'] = floats[16:19]
    data_dict['force'] = force_dict
    data_dict['moment'] = moment_dict
    return data_dict

time = []
drag = []
lift = []
moment = []

with open(forces_file,"r") as datafile:
    for line in datafile:
            if line[0] == "#":
                    continue
            data_dict = line2dict(line)
            time += [data_dict['time']]
            drag += [data_dict['force']['pressure'][0] + data_dict['force']['viscous'][0]]
            lift += [data_dict['force']['pressure'][1] + data_dict['force']['viscous'][1]]
            moment += [data_dict['moment']['pressure'][2] + data_dict['moment']['viscous'][2]]
datafile.close()

outputfile = open(testCaseName+'.txt','w')
for i in range(0,len(time)):
    outputfile.write(str(time[i])+' '+str(lift[i])+' '+str(drag[i])+' '+str(moment[i])+'\n')
outputfile.close()
```

Free surface profile data to dictionaries

```
#!/usr/bin/python

import os

os.chdir('../openfoam/___')
testCaseName = "___"
time = "___"

freeSurface_file = testCaseName+"/postProcessing/freeSurface/"+time+"/alpha.water_freeSurface.raw"

def line2dict(line):
    tokens_unprocessed = line.split()
    tokens = [x.replace(" ","").replace(" ","") for x in tokens_unprocessed]
    floats = [float(x) for x in tokens]
    coords = {}
    coords['x'] = floats[0]
    coords['y'] = floats[1]
    return coords

x = []
y = []

with open(freeSurface_file,"r") as datafile:
    for line in datafile:
            if line[0] == "#":
                    continue
            coords = line2dict(line)
            x += [coords['x']]
            y += [coords['y']]
datafile.close()

outputfile = open(testCaseName+'_'+time+'.txt','w')
for i in range(0,len(x)):
    outputfile.write(str(x[i])+' '+str(y[i])+'\n')
outputfile.close()
```